Wang, Dong; Schaaf, Peter

Plasmonic nanosponges

Original published in:
Advances in Physics: X : APX, ISSN 2374-6149, ZDB-ID 2889082-6. - Abingdon : Taylor & Francis Group. - 3 (2018), 1, art. 1456361, 19 pp.

Original published: 2018-03-28
ISSN (online): 2374-6149
DOI: 10.1080/23746149.2018.1456361
URL: https://doi.org/10.1080/23746149.2018.1456361
[*Visited:* 2018-04-20]

ADVANCES IN PHYSICS: X, 2018
VOL. 3, NO. 1, 1456361
https://doi.org/10.1080/23746149.2018.1456361

Taylor & Francis
Taylor & Francis Group

REVIEW ARTICLE

OPEN ACCESS Check for updates

Plasmonic nanosponges

Dong Wang and Peter Schaaf

Fachgebiet Werkstoffe der Elektrotechnik, Institut für Werkstofftechnik und Institut für Mikro- und Nanotechnologien MacroNano®, TU Ilmenau, Ilmenau, Germany

ABSTRACT

Gold nanosponges, or nanoporous gold nanoparticles, possess a percolated nanoporous structure over the entire nanoparticles. The optical and plasmonic properties of gold nanosponges and its related hybrid nanosponges are very fascinating due to the unique structural feature, and are controllable and tuneable in a large scope by changing the structural parameters like pore/ligament size, porosity, particle size, particles form, and hybrid structure. The nanosponges show the strong polarization dependence and multiple resonances behavior. Besides, the nanosponges exhibit a significantly higher local field enhancement than the solid nanoparticles. Strong nonlinear optical properties are confirmed by their high-order photoemission behavior, whereby long-lived plasmon modes are also clearly observed. All this is very important and relevant for the applications in enhanced Raman scattering, fluorescence manipulation, sensing, and nonlinear photonics.

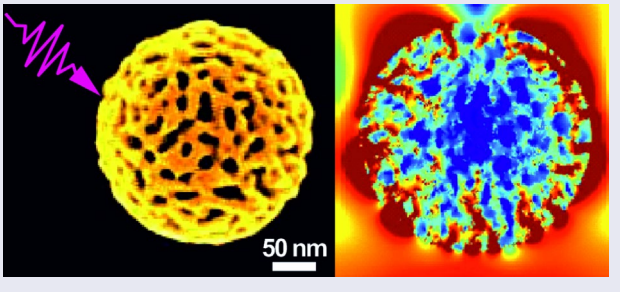

ARTICLE HISTORY
Received 26 October 2017
Accepted 19 March 2018

KEYWORDS
Nanosponge; nanoporous; hybrid; plasmonic; nonlinear optics

PACS
Optical properties of nanoporous materials, 78.67.Rb; collective excitations, 73.20.Mf; quantum optics, 42.50.-p; dynamics of nonlinear optical systems, 42.65.sf

CONTACT Dong Wang dong.wang@tu-ilmenau.de

1. Introduction

Nanoporous gold (NPG) has attracted increasing attentions due to its unique 3D bi-continuous ligament–channel structure with large specific surface areas for the applications in catalysis [1–3] and sensors [4]. Besides that, it has been also demonstrated that NPG can be used for biomolecules sensing with high sensitivity via surface enhanced Raman spectroscopy (SERS) due to its high surface-to-volume ratio together with its exceptional plasmonic properties [1,5,6]. NPG is usually formed by dealloying (selective leaching) of Au–Ag alloys, and during the dealloying process, the less noble element Ag is removed and the nanoporous structure of Au is formed. Some recent advanced research on nanoporous gold has been summarized in the book 'Nanoporous Gold: From an Ancient Technology to a High-Tech Material' [7].

The optical and plasmonic properties of the NPG are quite interesting. After dealloying, the color is changed from a shiny luster of Au–Ag alloy to dark dullness of NPG, because the light is scattered out by the nanoporous structure. Actually, the application of NPG in optical sensing is mainly based on its plasmonic properties. Surface plasmon resonances (SPR), the resonant oscillation of conduction electrons can be excited by the incident light at the surface of metals or the interface between metal and dielectrics. Depending on the structure of metals, either propagating mode in thin films or localized mode in nanoparticles can be excited. It is interesting to notice that simultaneous excitation of both propagating and localized surface plasmon resonances can be observed in the NPG membranes [8,9]. The plasmonic properties are tuneable by changing the porosity or volume fraction [10] and pore/ligament size [5,11]. The percolated porous structure with nanometer-sized ligaments can be considered as wonderful medium for the excitation of hot spots where the local field can be largely enhanced [11,12]. This is relevant for the application of SERS in which the nonlinear optical processes are strongly amplified [13,14]. This is also relevant for the enhancement of fluorescence [15]. Furthermore, strongly enhanced nonlinear light scattering, such as second-harmonic generation (SHG) scattering, has also been experimentally observed [16].

Recently, NPG has been fabricated in hierarchically nanostructured forms by combining the dealloying with the advanced nanostructuring technologies. For instance, NPG can be fabricated in the form of nanoparticles or nanosponges after dealloying of Au–Ag alloy nanoparticles [17]. The optical and plasmonic properties (especially, the localized plasmon resonances) of the nanosponges are even more fascinating due to the distinct structural feature, in which both 3D character of the porous (percolated air/gold) structure and 0D character of nanoparticle form are well integrated and combined. Besides, the limited sponge or particle size enables the optical characterization in a more convenient way.

In this short review, we survey the recent research work on the nanosponges. After describing their fabrication, the distinct plasmonic properties are reported.

In addition to the large enhancement of local field, the gold nanosponges also exhibit a large tuneability of plasmonic resonances from visible to NIR range by controlling the porosity, particle size, particle form, and pore/ligament size [18–20]. The plasmonic properties can be tuned further by forming the structure of hybrid nanosponges [18,21]. The nanosponges show strong polarization dependence due to the structural anisotropy contributed from the constraint of the nanoporous structure within a limited nanosponge or particle size [22,23]. Strong nonlinear optical behavior and even long-lived plasmon modes can be also observed in the gold nanosponges [24], which can be therefore used as efficient nanoantenna for many spectroscopic and sensing applications.

2. Fabrication

2.1. Fabrication of nanoporous gold

The most popular method for the fabrication of nanoporous gold is via dealloying of a gold-poor alloy containing a less noble element (such as silver). During the dealloying process, the less noble element is removed and the porous structure of gold is formed [25]. Actually, this method has already been used as the technique for 'depletion gilding' throughout the centuries in Europe [26,27]. However, the porous structure was identified for the first time using transmission electron microscopy (TEM) till to 1963 [28].

Different alloys, such as Au–Ag [26], Au–Cu [29] and Au–Al [30], can be used as starting materials for the generation of NPG. Dealloying can be performed by both chemical and electrochemical ways. For the chemical way, nitric acid is usually used, and the element Ag can be removed from the alloy by the acid. For the effective dealloying, the composition of Ag in the alloy must be beyond the so-called 'parting limit' of around 55% [3,31]. Alternatively, an anodic potential can be applied for the electrochemical dealloying. Here, the important thermodynamic parameter is the critical potential which is the threshold potential for dealloying and dependent on the composition of the alloy, the electrolyte and the further additives [32]. Pore/ligament size can be tuned by changing the dealloying conditions (such as solution concentration, dealloying time, and temperature), and vary from around 10 nm to over micron [12,33]. The ligaments possess the morphology of coexistent concave and convex with high curvature gradients, which enable the porous structure highly active by the catalytic applications [34]. Porous gold with multilevel porous structures can be also realized by applying a two-step dealloying strategy [35]. Residual Ag can be often detected in the NPG formed from Au–Ag alloy. Macroscopic volume shrinkage (by up to 30%) is also often observed due to the generation of a large number of lattice defects and local plastic deformation during dealloying [36]. The volume contraction leads usually to the formation of cracks in the NPG, but the crack formation can be also avoided by modification of the dealloying conditions [37].

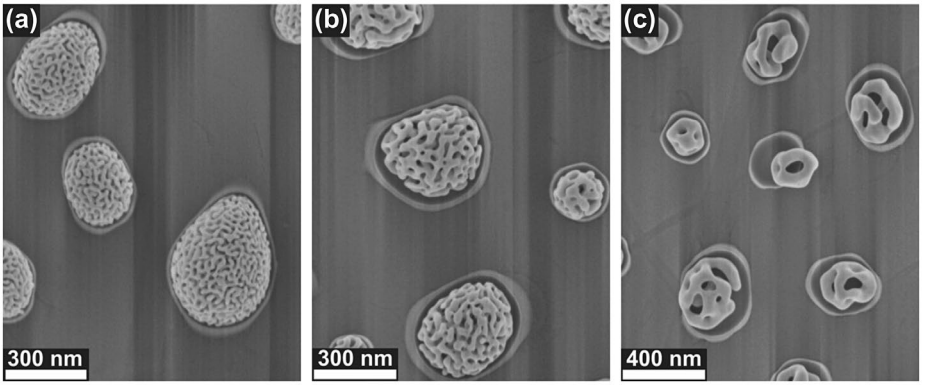

Figure 1. SEM images of gold nanosponges with different mean ligament/pore sizes: (a) 11.6 nm/9.0 nm, (b) 22.8 nm/14.4 nm, and (c) 50.4 nm/32.7 nm. Reproduced from Ref. [18] with permission from American Chemical Society.

2.2. Fabrication of gold nanosponges and hybrid nanosponges

By combining with other synthesis or nanofabrication methods including polyol process, templated process, solid-state dewetting, and different nanolithography techniques, Au–Ag alloys can be formed in many specific forms, and after dealloying, the nanoporous gold can be obtained in the corresponding forms, including the forms of nanotubes [38], nanowires [39], nanoparticles [17,40,41], hollowed nanospheres [42], nanobowls [43], nanodisks [44,45], ordered array of nanoparticles and nanodisks [46–48].

For instance, Figure 1 shows the scanning electron microscopy (SEM) images of the gold nanosponges (nanoporous gold nanoparticles) which are formed via thermal annealing induced solid-state dewetting of Au/Ag bi-layers and a subsequent dealloying process [17]. Solid-state dewetting is a phenomenon of instability of thin metal films driven by reduction of surface energy. The solid-state dewetting occurs via atom diffusion at the temperatures below melting point of the films, and can be used as self-assembly method for the fabrication of metallic nanoparticles [49–55]. Au–Ag alloy nanoparticles are formed after the solid-state dewetting of Au/Ag bi-layers. According to the principle of 'parting limit', the thickness ratio between Au and Ag layers should be small so that Ag-rich alloy nanoparticles can be formed for the effective dealloying. Then during the dealloying, Ag is removed from the particles and gold nanosponges are formed. The porous structure is actually over the entire individual nanosponges, as shown in the cross-sectional transmission electron microscopy (TEM) image in Figure 2(a). It is also interesting to notice that the individual nanosponges are single crystalline, as indicated by the points signal in the electron diffraction image of Figure 2(b). The rings signal is from the Pt which was deposited as protection layer prior to milling the nanosponge using focused ion beam (FIB).

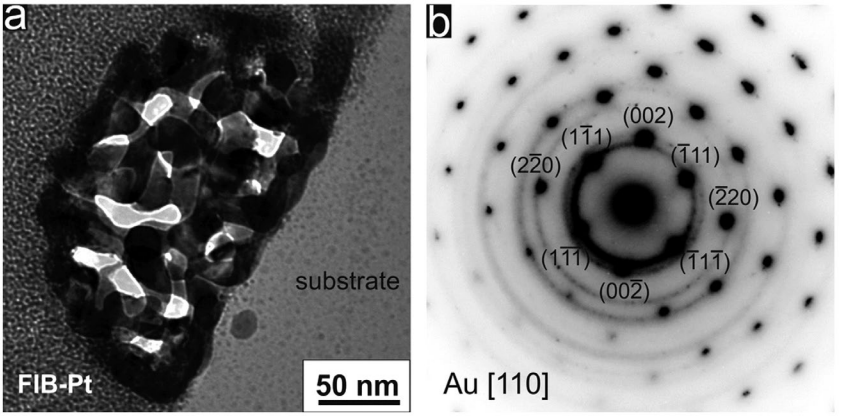

Figure 2. (a) Cross-sectional TEM images of a gold nanosponges, and (b) the corresponding selected area electron diffraction (SAED) image. Reproduced from Ref. [18] with permission from American Chemical Society.

The mean particle size can be varied from around 50 nm to micron range by changing the total layer thickness of the bilayers for the dewetting process. The mean ligament/pore size can be also tuned via two different approaches. One is by changing the dealloying conditions, such as temperature, concentration of nitric acid, and dealloying time. Figure 1 shows the SEM images of gold nanosponges, where the ligament/pore sizes increase with increasing temperature and concentration of nitric acid [18]. An alternative approach is based on annealing induced coarsening of the as-dealloyed nanosponges [56]. The onset temperature for coarsening is about 160 °C. The structural evolution by coarsening is largely dependent on the annealing temperature and pressure. During the coarsening, the small pores collapse initially very fast, and then this is followed by a stable stage of the coarsened structure at a constant temperature. The coarsening kinetics was recently well studied [56–58]. The details about the statistic analysis of the particle size, pore size, and ligament size can be found in the Ref. [18].

Furthermore, by employing the nanolithography techniques, periodically ordered arrays of gold nanosponges can be obtained, as shown in Figure 3. Here, a pre-patterned substrate with pyramidal pits array was fabricated using nanoimprint lithography, and subsequently used for the solid-state dewetting of Au/Ag bilayers. Ordered array of Au–Ag alloy nanoparticles were formed by thermal annealing induced solid-state dewetting. The mechanism of formation of the particles array is related to the Gibbs–Thomson effect [51,59], which describes the dependence of an excess local chemical on the local curvature. When the curvature driven diffusion dominates in the process for the optimized total bilayer thickness, the periodic modulation of the chemical potential through the periodic change in local curvature leads to the formation of the periodic array of the nanoparticles. Then, the Ag has been removed and the ordered array of gold nanosponges was formed after dealloying.

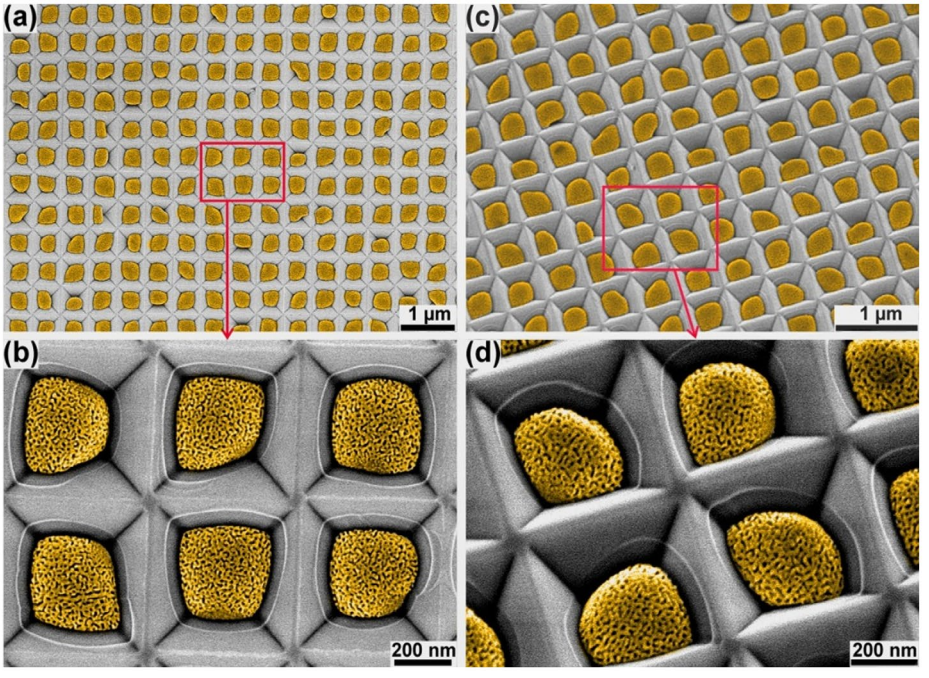

Figure 3. SEM images of ordered arrays of nanoporous gold nanoparticles. Reproduced from Ref. [46] with permission.

It is well known that different functionalities, including optical [60–62], magnetic [63], and catalytic properties [64], can be effectively enhanced by the hybridization effect of the bimetallic nanostructures. Bimetallic nanosponges and even hybrid nanosponges can be also achieved. For instance, it has been demonstrated that Au–Ag alloy nanosponges with SiO_2 shell possess the superior SERS activities [65]. There is a clear redshift of the plasmonic resonance for the Au/Al_2O_3 hybrid nanosponges comparing to the gold nanosponges [18], and the thermal stability of the gold nanosponges has been clearly enhanced by the hybrid structures [66].

Furthermore, Au/Ag hybrid nanosponges can be also obtained by using cyclic electroless deposition of Ag into the porous structure of the as-prepared gold nanosponges [21]. The amount of Ag in the hybrid nanosponges can be well controlled by the cycle number of the electroless deposition, and thereby, the porosity decreases upon the cycle number. In the Au–Ag alloy nanosponges, which are formed from incomplete dealloying of well-mixed Au–Ag alloy nanoparticles, both elements Au and Ag are mixed at atomic level. But in the Au/Ag hybrid nanosponges, both Au and Ag components are mixed at mesoscale size, as schematically shown in Figure 4(f). The optical properties of the Au/Ag hybrid nanosponges are also different from those of gold nanosponges. In addition to plasmon resonance peak of Au, there is also a clear peak of Ag, as seen in Figure 4(g). The plasmonic spectra were obtained by the ensemble measurement using UV–vis–NIR spectrometer. Both peaks of Au and Ag shift blue with decreasing

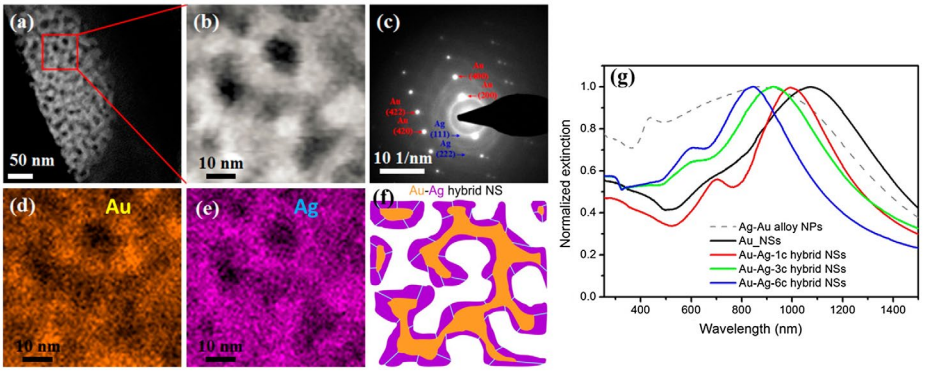

Figure 4. (a, b) STEM high angle annular dark field (HAADF) image; (c) SAED image; (d) Au mapping; (e) Ag mapping; (f) schematic 2D drawing of the hybrid structure with single-crystalline Au and polycrystalline Ag; and (g) Extinction spectra of gold nanosponges (NSs) and the Au/Ag hybrid nanosponges with mean particle size of 393 nm (1c, 3c, and 6c indicate different amount of Ag in the hybrid nanosponges. The spectrum of the Au–Ag alloy nanoparticles (NPs) before dealloying is also included for comparison. Reproduced from Ref. [21] with permission from American Chemical Society.

porosity (or increasing amount of Ag). Furthermore, the Au/Ag hybrid nanosponges show a clearly enhanced SERS performance for detection of butter yellow than the gold nanosponges [21].

3. Distinct plasmonic properties of the nanosponges

3.1. Large tuneability of localized surface plasmon resonances

The localized surface plasmon resonances (LSPR) of gold nanosponges can be tuned over a much broader spectral range than that of their solid counterparts, as shown in Figure 5. Figure 5 shows the extinction spectra of both Ag–Au alloy nanoparticles (NPs) and gold nanosponges or nanoporous gold nanoparticles (NPG-NPs) with different mean particle sizes (D). The spectra were obtained by the ensemble measurement using UV–vis–NIR spectrometer. In spite of the difference in LSPR between Au–Ag alloy NPs and Au solid NPs, the large red shift of the LSPRs due to the porous structure can be clearly observed. The plasmon resonances are clearly shifted in the near infrared (NIR) range. The effect of the nanoporosity on plasmon resonances is very obvious. Generally, the resonance peak of the nanosponges is sharper than that of the solid nanoparticles. However, the resonance peak of the small nanosponges (D = 54 nm) is broader than that of the same-sized solid nanoparticles probably due to the strong polarization effect (more details in Section 3.2).

It is also clearly observed in Figure 5, that the LSPR of the gold nanosponges red shifts with increasing particle size, and so there is a joint effect of particle size here. In order to explore the influence of the nanoporosity and the joint particle size effect in depth, simulations based on finite-difference time-domain (FDTD)

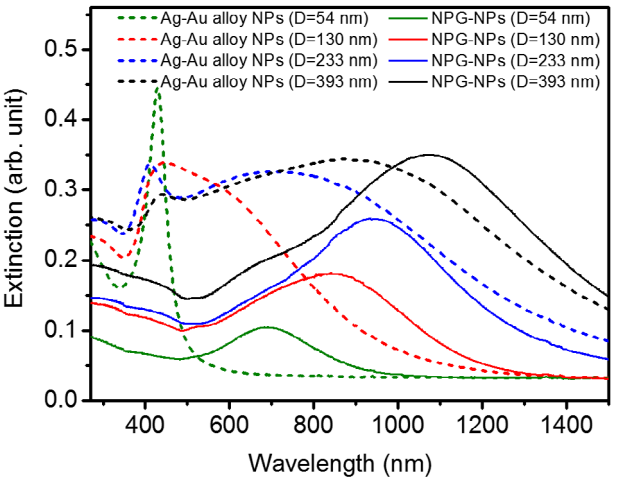

Figure 5. UV–vis–NIR extinction spectra of the Ag–Au alloy NPs (dashed lines) and the corresponding NPG-NPs (solid lines) with different mean particle sizes (*D*). Reproduced from Ref. [18] with permission from American Chemical Society.

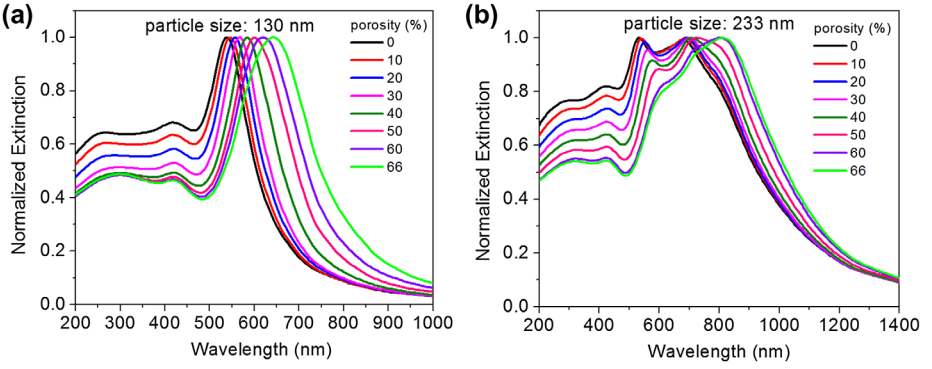

Figure 6. Calculated extinction spectra of the spherical gold nanosponges with various volume porosities: (a) small particle size (diameter) of 130 nm, and (b) large particle size of 233 nm. Reproduced from Ref. [18] with permission from American Chemical Society.

method have been performed. The exact micorstructure of the nanosponges is very complex and a precise model with percolated porous structure for the simulation is very difficult to construct. A simplified model was constructed with a gold sphere etched by N randomly distributed spherical air pores [18,20,21]. Volume overlap is allowed between the air pores for the representation of the percolated structure. The porosity can be determined by the number of the air pores. Figure 6 shows the simulated extinction spectra as a function of volume porosity for two different particle sizes. The plasmon peaks red shift with increasing porosity for both particle sizes. However, the influence of the nanoporosity is also clearly dependent on the particle size itself. For the small particle size, the dipole resonance peak becomes broader with increasing porosity, and this is probably due to the strong

polarization effect of the porous structure that will be discussed in next subsection. For the large solid particles, the quadrupole mode is more obvious. However, the peak of the quadrupole mode becomes weaker with increasing porosity. All this suggests that the effect of nanoporosity is very complicated, and together with the joint particle size effect bestows the nanosponges a large tuneability of the plasmonic properties.

3.2. Multiple plasmon resonances and polarization dependence

The information about the plasmonic resonances shown in Figure 5 was averaged information of many nanosponges obtained from the ensemble measurements with UV–vis–NIR spectrometer. In order to get a more deeper insight on the optical behavior and properties experimentally, Vidal et al. have perfomred the measurements of single particle order single nanosponge spectroscopy, and revealed that the optical properties of the individual nanosponges are much more complicated than those of their solid conterparts [22]. The plasmon renonance of the individual gold nanosponges with similar form, size, porosity, and ligament/pore size differs notably from each other. This means that the plasmonic spectra are unique to each nanosponge due to the individual porous configuration.

Furthermore, the gold nanosponges demonstrate an interesting and strong polarization effect [22,23]. Figure 7 shows the SEM images of two individual gold nanosponges and the corresponding polarization-dependent scattering spectra. Multiple plasmonic resonances can be even resolved when the polarizer is applied, implying that the individual nanosponges are actually multi-colored. Again, the polarization dependence is unique to each nanosponge due to unique individual porous configuration. Such multiple plasmonic contribution arises from localized plasmon resonances of the Au filaments and coupling between these resonances throughout the nanosponge. The spectra of the plasmonic eigenmodes of each nanosponge, resolved by the polarized light, are clearly sharper than the averaged overall spectra. The sharp spectra of the plasmonic eigenmodes indicate that the losses are not very pronounced. It has been further revealed by FDTD simulation that the strong polarization dependence vanishes when the particle becomes solid [22]. This could be the explanation why the overall plasmonic peak of the small nanosponges ($D = 54$ nm) becomes broader with increased porosity (Figure 6(a)). With increased porosity, the behavior of multiple resonances shows up and the overlap or composition of the multiple resonances leads to broadening of the overall spectrum. It is also clear here that due to the limited particle or sponge size (especially, when the particle size is clearly smaller than the wavelength of the light), the percolated air/gold structure in the individual nanosponges cannot be treated as a homogeneous effective medium. In other words, the structural anisotropy becomes more predominant due to the limited particle size, leading to the anisotropic optical behavior (polarization dependence of the scattering). Every

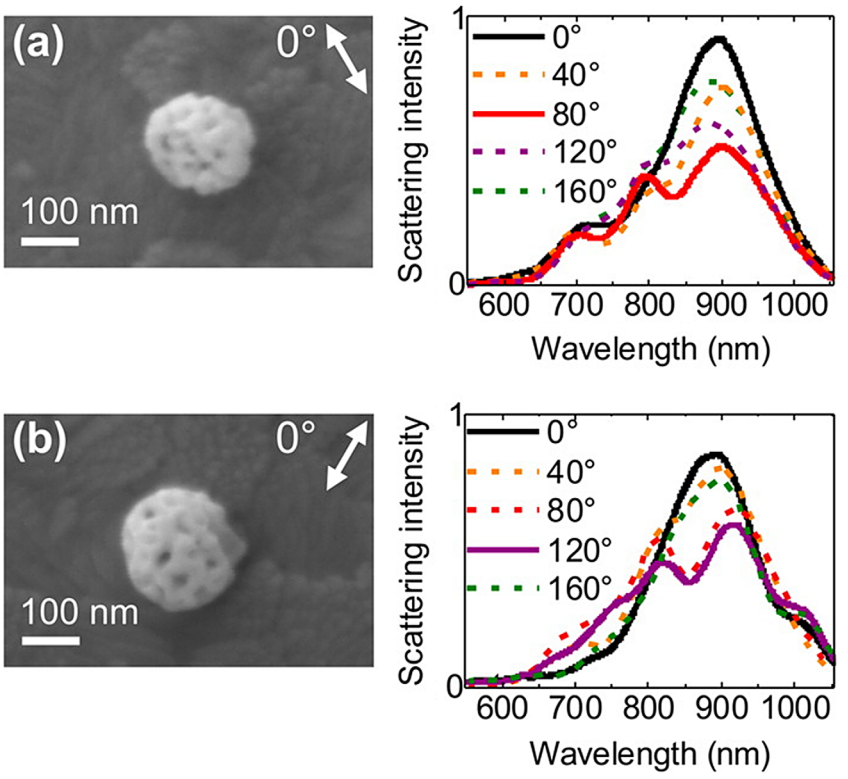

Figure 7. SEM images (left) and polarization-dependent scattering spectra (right) of (a) a 195-nm nanosponge and (b) a 220-nm nanosponge. The double arrows in the SEM images represent the 0° polarization axis. The polarizer axis was rotated clockwise in 20° steps but, for clarity, only 40° steps are shown here. Reproduced from Ref. [22] with permission from American Chemical Society.

nanosponge possesses an unique anisotropic feature due to its unique individual porous configuration.

The photoluminescence (PL) of bulk gold is resulted from the recombination of an electron excited from d-band into sp-band and the generated and scattered hole, and the PL emission has an extreme low efficiency with a quantum yield of 10^{-10} [67]. By comparison, nanostructured gold, for instance, gold nanoparticles, shows a more efficient radiative emission with enhanced quantum efficiency of many orders of magnitude attributed to the excitation of localized plasmons [68,69]. In other words, electron–hole recombinations can be practically localized by exciting a plasmonic hot spot, which will decay radiatively with enhanced quantum yield. Recently, both polarization-dependent scattering and PL of the same individual gold nanosponges with different particle or sponge size have been studied for comparison [23]. Figure 8(a)–(c) shows the polarization-dependent scattering spectra of three individual nanosponges with increasing particle or sponge size. The insets are the corresponding SEM images. All the three nanosponges show a strong polarization denpendence of scattering. The corresponding

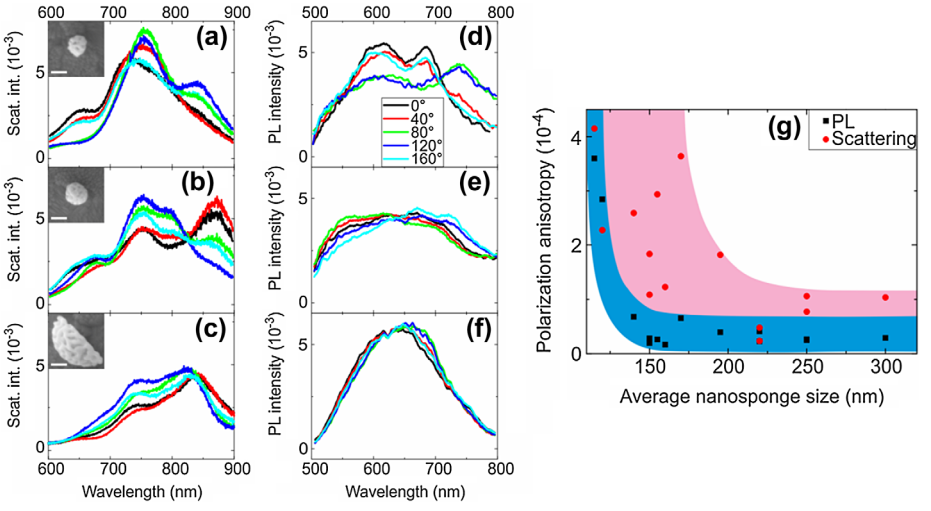

Figure 8. SEM images (scale bars 100 nm) and polarization-dependent scattering spectra of gold nanosponges, two almost spherical with diameters of 115, and 155 nm (a, b, respectively) and one with lateral dimensions of 410 and 195 nm (c). (d)–(f) Corresponding PL spectra of the same individual nanosponges. The legend in (d) gives the color coding of the polarization, valid for all panels. (g) Polarization anisotropy for scattering and PL of the individual Gold nanosponges. Reproduced from Ref. [23] with permission from American Physical Society.

polarization dependent PL spectra of the three nanosponges are shown in Figure 8(d)–(f). For the small nanosponge (Figure 8(a) and (d)), the strong polarization dependence of scattering is followed by the clear polarization dependence of PL, and the PL has an overall blue shift. For the large nanosponge (Figure 8(c) and (f)), the polarization dependence of PL is largely diminished, but it is still clear in the scattering specta. For the further quantitative comparison of the polarization dependence between the scattering and the PL spectra of the individual nanosponges, the degree of the polarization anisotropy, A, can be calculated as:

$$A = \int_{(x-150)\text{nm}}^{(x+150)\text{nm}} (I(80°) - I(0°))^2 d\lambda \tag{1}$$

where λ is the wavelength, and $I(\theta)$ are the polarization-dependent scattering or PL spectra at the polarization angle θ. Large integration window of 300 nm around each peak at x nm is taken so that the major spectral emission was covered in each case. Further details of the calculation can be seen in Ref. [23].

Here, it can be seen that the degree of polarization anisotropy is dependent on particle or sponge size, and somehow different between scattering and PL. The degree of polarization anisotropy of 14 individual gold nanosponges has been quantified and summaried in Figure 8(g). The polarization anisotropy of both scattering and PL decreases with increasing particle or sponge size. This is clear because the structural anisotropy becomes weakend with increasing particle size.

When the particle size is large enough, the percolated air/gold structure can be considered as a homogeneous effective medium, just like the nanoprous gold bulk samples. In addition, it is important to notice that the PL anisotropy ceases much faster with increasing particle size than scattering anisotropy. Clear polarization dependence of PL can be observed only in the nanosponges with particle size smaller than 120 nm, while strong polarization dependence of scattering can be even seen in the nanosponges with size of 200 nm.

The elctron–hole recombination can be actually considered as a point-like dipole light source inside of a nanosponge, which is characterized by the PL signal. The feature of the polarization-dependent scattering spectra is however yielded from the excitation by a plane wave from outside of the nanosponges. The difference of the polarization anisotropy between PL and scattering shown in Figure 8 indicates that the excitations of localized plasmons by the two different sources from outside and inside, are clearly different. In order to investigate the difference in depth, FDTD simulation has been performed [23]. As shown in Figure 9, three gold nanosponges with increasing particle size have been excited by both plane wave from outside (Figure 9(a)) and dipole from inside (Figure 9(b)), respectively. For the small nanosponge, similar distribution of excited hot spots over the whole nanosponge can be seen for excitations from both sources (Figure 9(c) and (d)). However, for the larger nanosponges, hot spots through the whole nanosponge can be still excited by the plane wave from outside but not by dipole from inside. This is even more pronounced for the largest nanosponge shown in Figure 9(g) and (h). So, it is clearly different from the case of plane wave excitation, that a plasmonic horizon with finite distance of about 57 nm is formed via local excitation from inside the nanosponge [23].

3.3. Nonlinear optical behavior and long-lived plasmon modes

The optical properties of the individual gold nanosponges have been further studied by performing ultrafast photoemission experiments with pulsed laser (pulse duration of 16 fs) at wavelength of 1600 nm [24]. Figure 10 shows the SEM image of five individual gold nanosponges and the corresponding photoelectron emission microscopy (PEEM) image, in which the photoemission of each nanosponge was clearly resolved.

Measurements of interferometric autocorrelation (IAC) were performed to study the time dynamics of the photoemission. Figure 11(a) shows the photoemission signal recorded from a single nanosponge as a function of the time delay Δt between the two pulses. By comparing the measured data (blue filled circles) with an instrument response (solid lines), it can be identified that the photoemission persists even for time delays of more than 40 fs, i.e. much beyond the time overlap of the two pulses. This means that the lifetime of the local electric field at the surface of the nanosponge was much longer than the duration of the incident laser field. Furthermore, photoemission is a strong nonlinear optical process. The

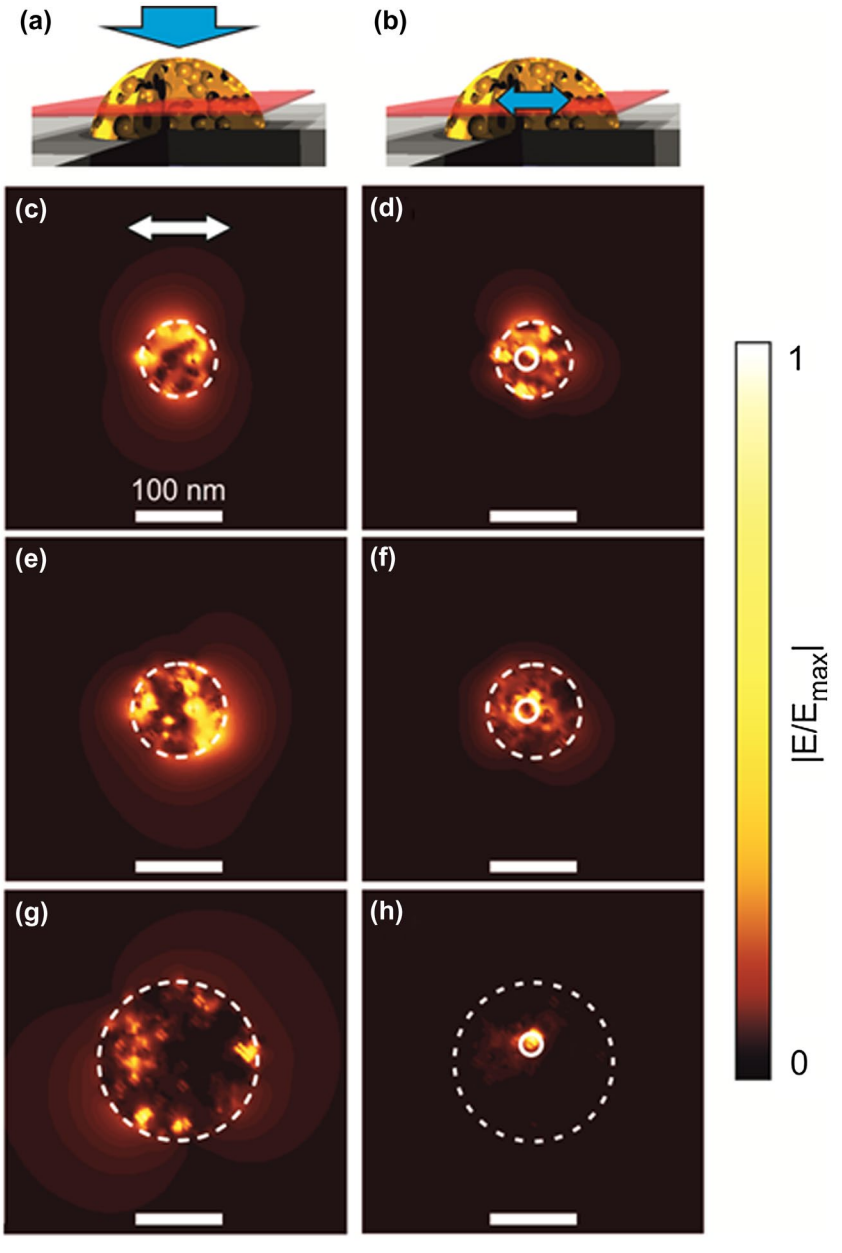

Figure 9. Numerically calculated distribution of the *E* fields through a cross section (red plane) inside gold nanosponges, excited by an external plane wave (scheme a, left column) or by an inside dipole (scheme b, right column). The diameters are 90 (c, d), 115 (e, f), and 195 nm (g, h). (c, e, g) Plane wave excitation, and (d, f, h) inside point dipole excitation. The dipole positions are indicated by small white circles. Reproduced from Ref. [23] with permission from American Physical Society.

nonlinearity of the emission process can be extracted from the autocorrelation tracing, and Figure 11(b) shows the plot of photoemission signal as a function of the maximum amplitude of the total incident laser field at the time delay for three

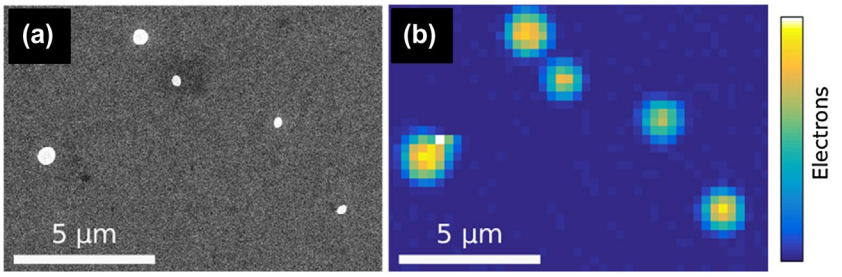

Figure 10. (a) SEM image of an overview of 5 gold nanosponges, and (b) photoelectron emission microscopy (PEEM) image of the same area of the sample with visible individual sponges. Obviously, all nanosponges show strong electron emission. Reproduced from Ref. [24] with permission from Nature publishing group.

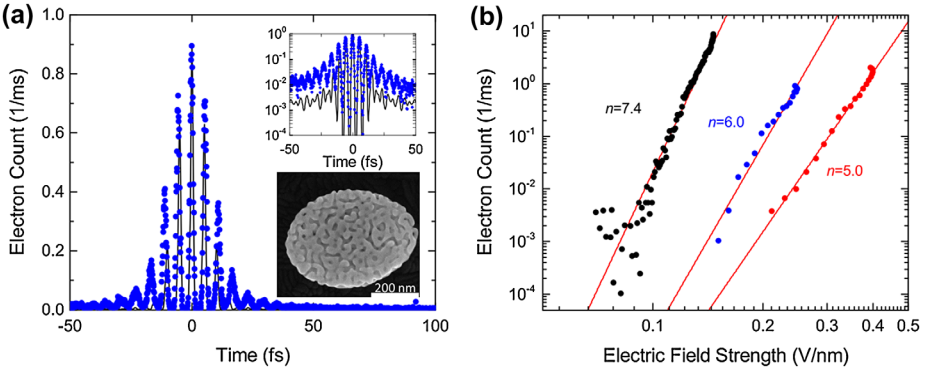

Figure 11. (a) Interferometric autocorrelation trace $C(\Delta t)$ of the photoemission from a single nanosponge (SEM image inset). The instrument response $C_0(\Delta t)$ simulated from the measured electrical field of the laser pulses $E_L(t)$ for a fifth order optical nonlinearity is shown as a solid line. The data are also represented on a logarithmic intensity scale (inset). (b) Optical nonlinearity of the photoemission deduced by plotting the recorded photoelectron signal from three representative nanosponges as a function of the maximum electric field amplitude of the laser pulses. Optical nonlinearities of order $n = 5\ldots7$ are deduced. Reproduced from Ref. [24] with permission from Nature publishing group.

individual gold nanosponges. The nonlinearity, n (the order of the multiphoton emission processes), is deduced from 5 to 7 for the three individual nanosponges, and well agreed with the estimation given by the ratio between the work function and the photon energy. This observed multiphoton emission behavior with high order of nonlinearity clearly indicates a high enhancement of local field at the surface of the nanosponges.

Furthermore, based on all these information, the lifetime of the localized hot spot can be deduced. In addition to the strong dipolar resonance mode with lifetime of 2.5 fs, the lifetime of the observed long-lived localized modes is around 10 times or even much more longer. The existence of the long-lived plasmon mode has been also confirmed by the results of the FDTD simulation [24], as

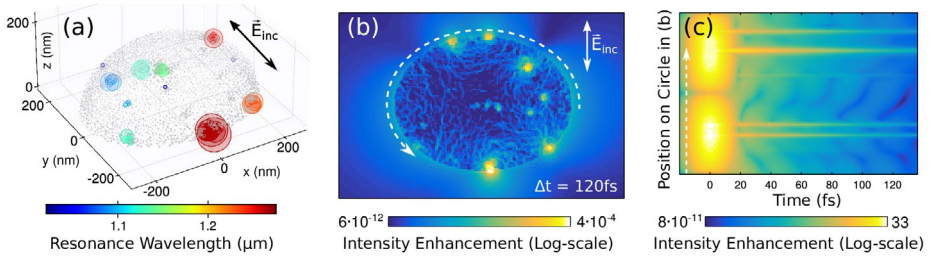

Figure 12. (a) Calculated intensity distribution and resonance wavelengths of localized modes with 10-nm pore size. The diameter of the circles corresponds to the amplitude of the dominating mode found by harmonic inversion at that specific point. The wavelength of the dominating mode is depicted by the displayed color code. (b) Local field intensity (logarithmic scale), calculated along a cross-cut through a plane parallel to the substrate, 5 nm above the substrate, and at a time delay of 120 fs after the arrival of the excitation pulse. (c) Time-dependent field intensity calculated along a circle close to the surface of the particle (see white dashed line in b). The y-axis gives the position on the circle. The maximum of the incident pulse is at 0 fs. Reproduced from Ref. [24] with permission from Nature publishing group.

shown in Figure 12. The coupling of far-field light to the short-lived dipolar mode of the nanosponge can lead to spatially delocalized surface plasmon polariton excitation, which can efficiently further couple the localized hot spots and make the localized hot spots long-lived. The different decay times for the delocalized short-lived dipolar and the long-lived localized modes can be clearly distinguished (Figure 12(c)). Furthermore, the calculation and simulation results show that a maximum enhancement of the local field intensity is found 40…45 times over that of the incident far-field, and the corresponding field enhancement factor is 6.7 [24]. Here, the gold nanosponges which exhibit highly field enhancement and long-lived hot spots, can be considered as robust nanoantennas for many interesting applications in the areas of manipulation of light and spectroscopic sensing, where incident far-field light can be efficiently captured and nonlinear processes can be largely enhanced.

4. Summary

Gold nanosponges are nanoporous gold in the form of nanoparticles, and possess a distinct structural feature, which combines both characters of 3D percolated porous network and 0D nanoparticle form. The optical and plasmonic properties of the nanosponges are very fascinating and can be well tuned and tailored through controlling the particle size, particle form, pore size and porosity. The porosity effect together with the joint particle size effect enables a large tuneability of the surface localized plasmon resonances, which can be even shifted to NIR range. Strong polarization effect and the behavior of multiple resonances can be observed in the individual gold nanosponges, indicating that the percolated porous structure within the limited particle size possesses a clear structural anisotropy and cannot be considered as a homogeneous effective medium. Both experimental observation

of multiple resonances and theoretical calculation have indicated that the gold nanosponges possess high density of hot spots with large field enhancement. But the direct experimental imaging of the hot spots in the nanosponges is still challenging. However, the strong field enhancement can be experimentally confirmed by the enhanced nonlinear optical behavior studied through light-induced electron emission. Furthermore, the time dynamics of electron emission with femtosecond time resolution is well studied using ultra-short laser pulse excitation, and long-lived plasmon modes have been revealed. Actually, the gold nanosponges can be considered as efficient nanoatennas where far-field light can be captured and localized. The distinct optical and plasmonic properties can be further modified by incorporating the second material component into the porous structure and forming the hybrid nanosponges. All these distinct optical properties of the plasmonic nanosponges can be essentially relevant for the applications in enhanced Raman scattering, fluorescence manipulation, sensing, and nonlinear photonics.

Acknowledgments

We are very grateful to Eszter Baradacs, Zoltan Erdelyi, Germann Hergert, Calin Hrelescu, Petra Groß, Thomas A. Klar, Leonid Klinger, Heiko Kollmann, Anna Kosinova, Christoph Lienau, Bence Parditka, Eugen Rabkin, Wenye Rao, Erich Runge, Felix Schwarz, Cynthia Vidal, Jan Vogelsang, Yong Yan, and Juemin Yi for ongoing collaborations and valuable discussions. The help of Joachim Döll, Birgitt Hartmann, Ilona Marquardt, Thomas Kups and Diana Rossberg in the sample preparation and characterization is gratefully acknowledged. We thank the Deutsche Forschungsgemeinschaft (DFG, SPP1839 'Tailored Disorder', grant SCHA 632/24) and the state of Thuringia (TMWAT, BioMacroNano2020, 2010-2012; Grant B715-10009) for financial support. We also acknowledge the support for the article processing charge by the German Research Foundation and the Open Access Publication Fund of the TU Ilmenau.

Disclosure statement

No potential conflict of interest was reported by the authors.

Funding

This work was supported by Deutsche Forschungsgemeinschaft [DFG, SPP1839 'Tailored Disorder', grant SCHA 632/24] and the state of Thuringia [TMWAT, BioMacroNano2020, 2010-2012; grant B715-10009].

ORCID

Dong Wang http://orcid.org/0000-0001-5940-9538

References

[1] Y. Ding and M. Chen, MRS Bull. 34 (2009) p.569.

[2] V. Zielasek, B. Jürgens, C. Schulz, J. Biener, M.M. Biener, A.V. Hamza and M. Bäumer, Angew. Chem. Int. Ed. 45 (2006) p.8241.
[3] A. Wittstock, J. Biener and M. Baumer, Phys. Chem. Chem. Phys. 12 (2010) p.12919.
[4] M. Hieda, R. Garcia, M. Dixon, T. Daniel, D. Allara and M.H.W. Chan, Appl. Phys. Lett. 84 (2004) p.628.
[5] M.C. Dixon, T.A. Daniel, M. Hieda, D.M. Smilgies, M.H.W. Chan and D.L. Allara, Langmuir 23 (2007) p.2414.
[6] L. Qian, B. Das, Y. Li and Z. Yang, J. Mater. Chem. 20 (2010) p.6891.
[7] A. Wittstock, J. Biener and M. Baumer, *Chapter 1 Introduction to Nanoporous Gold, in Nanoporous Gold: From an Ancient Technology to a High-Tech Material*, The Royal Society of Chemistry, London, 2012, p.1.
[8] F. Yu, S. Ahl, A.-M. Caminade, J.-P. Majoral, W. Knoll and J. Erlebacher, Anal. Chem. 78 (2006) p.7346.
[9] X.Y. Lang and M.W. Chen, *Chapter 6 Optical Properties and Applications of Nanoporous Metals, in Nanoporous Gold: From an Ancient Technology to a High-Tech Material*, The Royal Society of Chemistry, London, 2012, p.97.
[10] A.I. Maaroof, A. Gentle, G.B. Smith and M.B. Cortie, J. Phys. D: Appl. Phys. 40 (2007) p.5675.
[11] X.Y. Lang, L.Y. Chen, P.F. Guan, T. Fujita and M.W. Chen, Appl. Phys. Lett. 94 (2009) p.213109.
[12] L.H. Qian, X.Q. Yan, T. Fujita, A. Inoue and M.W. Chen, Appl. Phys. Lett. 90 (2007) p.153120.
[13] D.L. Jeanmaire and R.P. Van Duyne, J. Electroanal. Chem. Interfacial Electrochem. 84 (1977) p.1.
[14] M.G. Albrecht and J.A. Creighton, J. Am. Chem. Soc. 99 (1977) p.5215.
[15] L. Zhang, Y. Song, T. Fujita, Y. Zhang, M. Chen and T.-H. Wang, Adv. Mater. 26 (2014) p.1289.
[16] M. Breit, V.A. Podolskiy, S. Grésillon, G. von Plessen, J. Feldmann, J.C. Rivoal, P. Gadenne, A.K. Sarychev and V.M. Shalaev, Phys. Rev. B 64 (2001) p.125106.
[17] D. Wang and P. Schaaf, J. Mater. Chem. 22 (2012) p.5344.
[18] W. Rao, D. Wang, T. Kups, E. Baradács, B. Parditka, Z. Erdélyi and P. Schaaf, ACS Appl. Mater. Interfaces 9 (2017) p.6273.
[19] F. Schwarz and E. Runge, Ann. Phys. 529 (2017) p.1600234.
[20] Q. Zhang, N. Large, P. Nordlander and H. Wang, J. Phys. Chem. Lett. 5 (2014) p.370.
[21] Y. Yan, A.I. Radu, W. Rao, H. Wang, G. Chen, K. Weber, D. Wang, D. Cialla-May, J. Popp and P. Schaaf, Chem. Mater. 28 (2016) p.7673.
[22] C. Vidal, D. Wang, P. Schaaf, C. Hrelescu and T.A. Klar, ACS Photonics 2 (2015) p.1436.
[23] C. Vidal, D. Sivun, J. Ziegler, D. Wang, P. Schaaf, C. Hrelescu and T.A. Klar, Nano Lett. 18 (2018) p.1269.
[24] G. Hergert, J. Vogelsang, F. Schwarz, D. Wang, H. Kollmann, P. Groß, C. Lienau, E. Runge and P. Schaaf, Light: Sci. Appl. 6 (2017) p.e17075.
[25] J. Erlebacher, M.J. Aziz, A. Karma, N. Dimitrov and K. Sieradzki, Nature 410 (2001) p.450.
[26] Y. Ding, Y.J. Kim and J. Erlebacher, Adv. Mater. 16 (2004) p.1897.
[27] A.J. Forty, Nature 282 (1979) p.597.
[28] H.W. Pickering and P.R. Swann, Corrosion 19 (1963) p.373t.
[29] S. Kameoka, T. Tanabe, K. Miyamoto and A.P. Tsai, J. Chem. Phys. 144 (2016) p.034703.
[30] Z. Zhang, Y. Wang, Z. Qi, W. Zhang, J. Qin and J. Frenzel, J. Phys. Chem. C 113 (2009) p.12629.
[31] D.M. Artymowicz, J. Erlebacher and R.C. Newman, Philos. Mag. 89 (2009) p.1663.
[32] A. Dursun, D.V. Pugh and S.G. Corcoran, J. Electrochem. Soc. 150 (2003) p.B355.

[33] J. Biener, A.M. Hodge, J.R. Hayes, C.A. Volkert, L.A. Zepeda-Ruiz, A.V. Hamza and F.F. Abraham, Nano Lett. 6 (2006) p.2379.
[34] T. Fujita, P. Guan, K. McKenna, X. Lang, A. Hirata, L. Zhang, T. Tokunaga, S. Arai, Y. Yamamoto, N. Tanaka, Y. Ishikawa, N. Asao, Y. Yamamoto, J. Erlebacher and M. Chen, Nat. Mater. 11 (2012) p.775.
[35] Z. Qi, U. Vainio, A. Kornowski, M. Ritter, H. Weller, H. Jin and J. Weissmüller, Adv. Funct. Mater. 25 (2015) p.2530.
[36] S. Parida, D. Kramer, C.A. Volkert, H. Rösner, J. Erlebacher and J. Weissmüller, Phys. Rev. Lett. 97 (2006) p.035504.
[37] Y. Sun and T.J. Balk, Scr. Mater. 58 (2008) p.727.
[38] X. Gu, L. Xu, F. Tian and Y. Ding, Nano Res. 2 (2009) p.386.
[39] A. Chauvin, C. Delacôte, L. Molina-Luna, M. Duerrschnabel, M. Boujtita, D. Thiry, K. Du, J. Ding, C.-H. Choi, P.-Y. Tessier and A.-A. El Mel, ACS Appl. Mater. Interfaces 8 (2016) p.6611.
[40] X. Li, Q. Chen, I. McCue, J. Snyder, P. Crozier, J. Erlebacher and K. Sieradzki, Nano Lett. 14 (2014) p.2569.
[41] M.K. Khristosov, L. Bloch, M. Burghammer, Y. Kauffmann, A. Katsman and B. Pokroy, Nat. Commun. 6 (2015) p.8841.
[42] J. Biener, G.W. Nyce, A.M. Hodge, M.M. Biener, A.V. Hamza and S.A. Maier, Adv. Mater. 20 (2008) p.1211.
[43] S. Pedireddy, H.K. Lee, C.S.L. Koh, J.M.R. Tan, W.W. Tjiu and X.Y. Ling, Small 12 (2016) p.4531.
[44] G.M. Santos, F. Zhao, J. Zeng and W.-C. Shih, Nanoscale 6 (2014) p.5718.
[45] F. Zhao, J. Zeng, M.M. Parvez Arnob, P. Sun, J. Qi, P. Motwani, M. Gheewala, C.-H. Li, A. Paterson, U. Strych, B. Raja, R.C. Willson, J.C. Wolfe, T.R. Lee and W.-C. Shih, Nanoscale 6 (2014) p.8199.
[46] D. Wang, R. Ji, A. Albrecht and P. Schaaf, Beilstein J. Nanotechnol. 3 (2012) p.651.
[47] M.M.P. Arnob, F. Zhao, J. Li and W.-C. Shih, ACS Photonics 4 (2017) p.1870.
[48] D. Wang and P. Schaaf, Phys. Status Solidi (A) 210 (2013) p.1544.
[49] E. Jiran and C.V. Thompson, J. Electron. Mater. 19 (1990) p.1153.
[50] E. Jiran and C.V. Thompson, Thin Solid Films 208 (1992) p.23.
[51] A.L. Giermann and C.V. Thompson, Appl. Phys. Lett. 86 (2005) p.121903.
[52] D. Wang, R. Ji and P. Schaaf, Beilstein J. Nanotechnol. 2 (2011) p.318.
[53] D. Wang and P. Schaaf, Mater. Lett. 70 (2012) p.30.
[54] A. Herz, D. Wang, T. Kups and P. Schaaf, J. Appl. Phys. 116 (2014) p.044307.
[55] A. Herz, M. Friák, D. Rossberg, M. Hentschel, F. Theska, D. Wang, D. Holec, M. Šob, O. Schneeweiss and P. Schaaf, Appl. Phys. Lett. 107 (2015) p.073109.
[56] A. Kosinova, D. Wang, P. Schaaf, O. Kovalenko, L. Klinger and E. Rabkin, Acta Mater. 102 (2016) p.108.
[57] A.Y. Chen, S.S. Shi, F. Liu, Y. Wang, X. Li, J.F. Gu and X.F. Xie, Appl. Surf. Sci. 355 (2015) p.133.
[58] S. Kuwano-Nakatani, T. Fujita, K. Uchisawa, D. Umetsu, Y. Kase, Y. Kowata, K. Chiba, T. Tokunaga, S. Arai, Y. Yamamoto, N. Tanaka and M. Chen, Mater. Trans. 56 (2015) p.468.
[59] W.W. Mullins, J. Appl. Phys. 28 (1957) p.333–339.
[60] J. Chen, B. Wiley, J. McLellan, Y. Xiong, Z.-Y. Li and Y. Xia, Nano Lett. 5 (2005) p.2058.
[61] S. Kim, S.K. Kim and S. Park, J. Am. Chem. Soc. 131 (2009) p.8380.
[62] B. Chen, G. Meng, Q. Huang, Z. Huang, Q. Xu, C. Zhu, Y. Qian and Y. Ding, ACS Appl. Mater. Interfaces 6 (2014) p.15667.
[63] J.J. Schneider, Adv. Mater. 13 (2001) p.529.

[64] B. Lim, J. Wang, P.H.C. Camargo, M. Jiang, M.J. Kim and Y. Xia, Nano Lett. 8 (2008) p.2535.
[65] K. Liu, Y. Bai, L. Zhang, Z. Yang, Q. Fan, H. Zheng, Y. Yin and C. Gao, Nano Lett. 16 (2016) p.3675.
[66] A. Kosinova, D. Wang, E. Baradács, B. Parditka, T. Kups, L. Klinger, Z. Erdélyi, P. Schaaf and E. Rabkin, Acta Mater. 127 (2017) p.108.
[67] A. Mooradian, Phys. Rev. Lett. 22 (1969) p.185.
[68] M.B. Mohamed, V. Volkov, S. Link and M.A. El-Sayed, Chem. Phys. Lett. 317 (2000) p.517.
[69] G.T. Boyd, Z.H. Yu and Y.R. Shen, Phys. Rev. B 33 (1986) p.7923.